PHYSICAL REVIEW A VOLUME 35, NUMBER 1 JANUARY 1, 1987

Field-induced tetragonal blue phase (BP X)

P. Pieranski
Laboratoire de Physique des Solides, Université de Paris—Sud, Bâtiment 510, Centre d'Orsay, 91405 Orsay Cédex, France

P. E. Cladis
AT&T Bell Laboratories, 600 Mountain Avenue, Murray Hill, New Jersey 07974-2070
(Received 26 June 1986)

Hornreich *et al.* predicted that blue phases I, II, or III should undergo structural transformations into anisotropic uniaxial blue phases in electric or magnetic fields. It is shown here that, besides a hexagonal blue phase BP H^{3D} discovered previously, a novel blue phase, called BP X, can be obtained either from BP I for $\mathbf{E}||[110]$ or from BP II for $\mathbf{E}||[100]$. Using the method of Kossel diagrams, clear-cut evidence is presented that blue phase X has tetragonal symmetry. The transformation of BP I into BP X involves a homogeneous strain in the plane perpendicular to $\mathbf{E}$ and a dilation in the field direction.

I. INTRODUCTION

In cholesteric materials such as, for example, the extensively studied mixtures of a cholesterogene CB15 with a nematic liquid crystal E9, four different mesophases have been identified: (i) an amorphous blue phase III or "blue fog," BP III; (ii) cubic blue phase II of symmetry, O^2 ($P4_232$), BP II; (iii) cubic blue phase I of symmetry O^8 ($I4_132$), BP I; (iv) the usual helicoidal or cholesteric phase, C.

Theoretical studies of this cholesteric polymorphism have accounted for these four mesophases as well as other phases with different symmetries. In particular, Hornreich *et al.*[1] pointed out that cholesteric materials with positive dielectric anisotropy (such as mixtures of CB15 with E9) should exhibit uniaxial anisotropic phases in an electric field. This theoretical prediction was confirmed recently in Ref. 2 where the first evidence for a field-induced hexagonal phase was given.

The experimental results, concerning a mixture of 49.8% of CB15 in E9 (Ref. 2) differed, however, from the predictions of Hornreich *et al.* in two main points: (1) The observed phase (called H^{3D}) was three dimensional in contrast to the two-dimensional (2D) hexagonal phase considered in Ref. 1. (2) On the phase diagram (Fig. 1 in Ref. 2, temperature versus field) between the low-field BP II phase and the high-field H^{3D} phase, there was another phase, different from both BP II and H^{3D}. Since we could not exclude the possibility that this intermediate phase was BP I, we called it, by precaution and for the time being, BP X.

In this paper, we present clear-cut experimental evidence that the BP X of Ref. 2 is not cubic and therefore neither BP I or BP II, but a new blue phase with tetragonal symmetry. We deduced the structure of BP X from its Kossel diagrams, i.e., the diffraction patterns of monocrystals in a divergent light beam.

In Sec. II we report our new results concerning the conditions for the occurrence and microscopic observations of the BP X phase. In Sec. III we describe the experimental setup for the divergent beam technique and show Kossel diagrams of BP I and BP X phases. In Sec. IV we interpret Kossel diagrams of the BP X phase qualitatively (symmetry) and quantitatively (parameters of the tetragonal lattice).

II. CONDITIONS FOR THE OCCURRENCE OF THE BP X PHASE IN MIXTURES OF CB15 WITH E9

Before showing Kossel diagrams of the BP X phase obtained for the first time only recently, it is useful to describe other characteristic features of this new phase, accessible by direct observations in a metallurgical microscope with monochromatic illumination.[3]

The observations were made on several samples with concentrations c of CB15 in E9 ranging from 40% to 60%. The samples were introduced by capillarity into a cell made of two parallel glass plates S_b and S_u, coated with semitransparent In0 electrodes and separated by 30-μm Mylar spacers (Fig. 1). The bottom glass plate (S_b) was thin (≈ 0.15 mm) and in thermal contact, through immersion oil (IO), with a $40x$ objective. The objective was fixed on an aluminum piece P_1 whose temperature T_1 was regulated using Peltier-effect elements. The upper glass plate (3 mm thick) was pressed against an aluminum piece P_2 by two metallic, elastic lamellas (L_1,L_2) also used as electric contacts. The electrode of the bottom glass plate was connected by a conducting epoxy to the lamella L_2. The electrode of the upper plate was connected to L_1. The frequency of an ac voltage, applied to the cell through L_1 and L_2 was $f=10$ kHz. The temperature T_2 of the aluminum piece P_2 was regulated, independently of P_1, by other Peltier elements.

A. BP II→BP X, $46\% < c < 52\%$

Individual crystals of BP II can be nucleated and grown in the isotropic phase in samples where the concentration c is between 46% and 52%. As reported before,[2] when

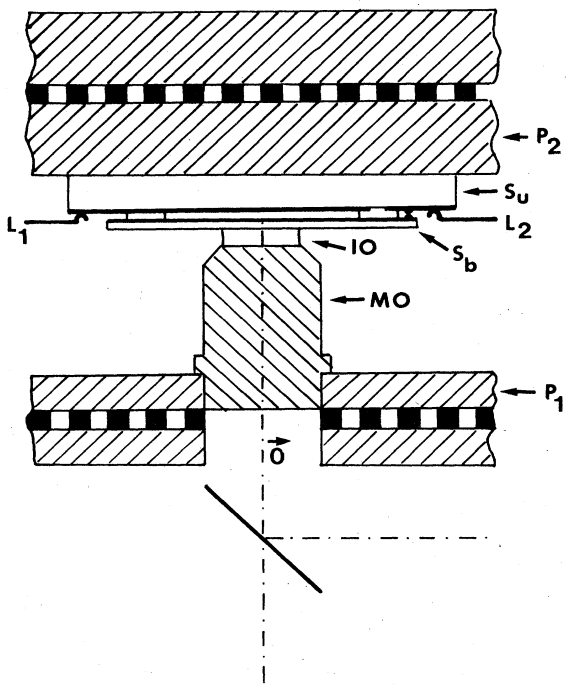

FIG. 1. Experimental cell.

the nucleation and growth take place in electric field E less than E_1 (E_1, following Ref. 2 is the critical field for the BP II→BP X transition) then all BP II crystals orient with their fourfold axes (for example, [001]) parallel to E. The wavelength $\lambda_{\mathrm{BP\,II}}^{[001]}(E)$ of circularly polarized Bragg reflection from (001) planes increases with increasing E as shown in Fig. 2. Heppke *et al.*[4] also observed this effect.

At $E=E_1$, a first discontinuity marks the transitions BP II→BP X while that at $E=E_2$ corresponds to the transition BP X→H^{3D}. As reported before,[2] the square shape of field oriented BP II crystals is preserved in the BP X phase. In the H^{3D} phase the crystals become hexagonal. In conclusion the discontinuity of the wavelength $\lambda^{[001]}(E)$ of the Bragg reflection from square-shaped crystals is the "fingerprint" of the BP II→BP X transition.

B. BP I→BP X, 42% < c < 46%

In samples where the concentration c of CB15 was less than 46%, BP I crystals, instead of BP II crystals, nucleate directly and grow in the isotropic liquid phase. BP I crystals that nucleated on the glass plates are oriented with their (110) or (211) planes parallel to them. When an electric field is applied to such surface-oriented crystals at $E=E_{I/x}$, the crystals with (110)$||S_b$ [Fig. 3(a)] undergo a drastic modification of their shapes, shown schematically in Fig. 3(b). This deformation involves a dilation along a [001] axis and compression along a [1$\bar{1}$0] axis. Figure 3 shows [001] and [1$\bar{1}$0] directions in the (x,y) plane perpendicular to the field (**E**||**z**). Consequently, the angle $\alpha=109.5°$ between (1$\bar{1}$2) and ($\bar{1}$12) facets becomes $\alpha'=90°$ [Fig. 3(c)]. When such field transformed crystals are grown by slowly cooling the sample, new facets (001) and (00$\bar{1}$) develop progressively [Fig. 3(d)], and the overall crystal shape turns to a square one [Fig. 3(e)].

It is interesting to note that the wavelength of the Bragg reflection from (110) planes parallel to S does not show a detectable discontinuity at BP I→BP X transition.

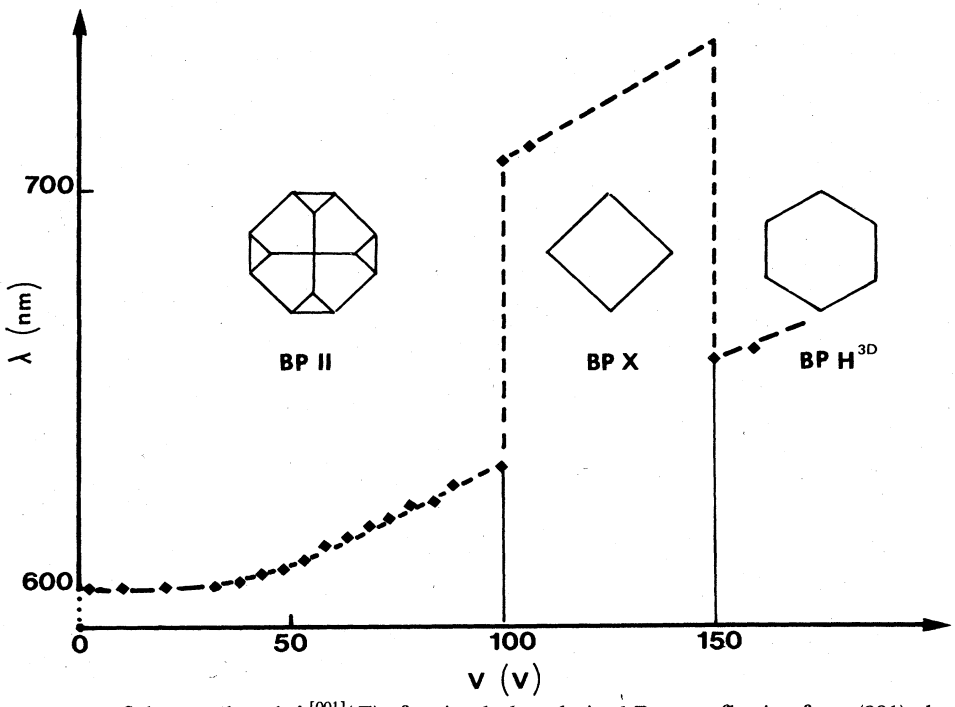

FIG. 2. Field dependence of the wavelength $\lambda_{\mathrm{BP\,II}}^{[001]}(E)$ of a circularly polarized Bragg reflection from (001) planes perpendicular to the field **E**.

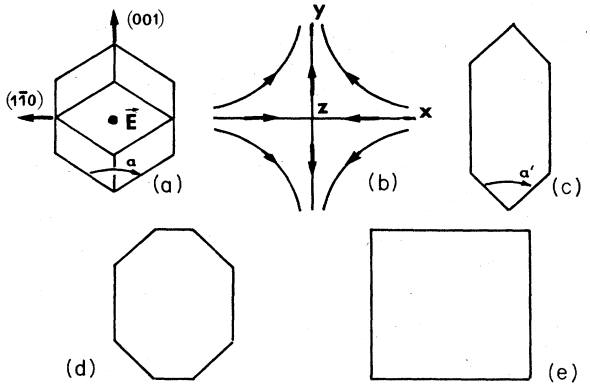

FIG. 3. Deformation of a BP I crystal in an electric field: (a) orientation of the crystal with respect to the field, (b) deformation of a crystal in the field, (c) shape of the crystal at $E = E_{I/X}$, (d) appearance of new crystal facets, (e) asymptotic shape of the BP X crystal growing in the field.

C. BP I→BP X, $c > 46\%$

Isolated crystals of BP I do not coexist with the isotropic liquid when there is a BP II phase. Instead many small crystallites of BP I touch each other to form a mosaic texture. The BP I→BP X transition cannot then be detected by direct observation of crystal shapes but it is marked by the disappearance of the so-called "cross-hatched patterns" characteristics of BP I crystals grown from blue phase II (Ref. 5). These patterns are made by parallel bands of twinned crystals with orientations shown in Fig. 4(a). Consider two adjacent strips such as T_1 and T_2. When simple shear deformations of opposite signs are applied to T_1 and T_2 [Fig. 4(b)], the rectangular cross sections of cubic unit cells [Fig. 4(a)] deform into the square cross sections of the quadratic unit cells of BP X. The irrotational part of the simple shear deformation is the same here as in the former case (see Fig. 3).

D. Conclusions

The above observations lead to the following conclusions concerning BP X.

(1) BP X has a fourfold helicoidal axis parallel to the field **E**.

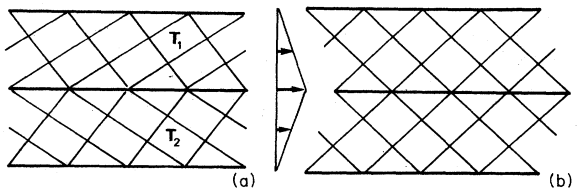

FIG. 4. Disappearance of the "cross-hatched pattern" at the BP I→BP X transition: (a) BP I, rectangular cross sections of the Bravais lattices in adjacent twins, (b) square cross section of the tetragonal Bravais lattice in BP X obtained by simple shear deformations shown by the arrows, and a small dilation perpendicular to the shear.

(2) BP X can be obtained from BP II when (a) crystals of BP II are oriented with their fourfold axis parallel to **E**, (b) E is larger than a threshold value E_1 (which depends on the composition of the sample).

(3) The BP II→BP X transition is marked by a discontinuity of the wavelength of Bragg reflection from (100) planes perpendicular to **E**.

(4) BP X can also be obtained from BP I when (a) crystals of BP I are oriented (for example, by surfaces) with their twofold axis parallel to **E**, (b) the field is larger than a threshold value $E_{I/X}$.

(5) Isolated BP I crystals deform macroscopically during the BP I→BP X transition, as shown in Fig. 3.

III. KOSSEL DIAGRAMS, EXPERIMENTAL

A. Principle of the convergent beam technique

Observations of crystal forms or other morphological details (facets, steps on facets, bulk dislocations, grain boundaries, twins in cross-hatched patterns, etc.) as well as measurements of the Bragg reflection from crystal planes (hkl) perpendicular to the axis **O** of the microscope were performed with the aperture diaphragm of the microscope closed. Under these conditions, the sample is illuminated by a collimated beam of rays parallel to **O**.

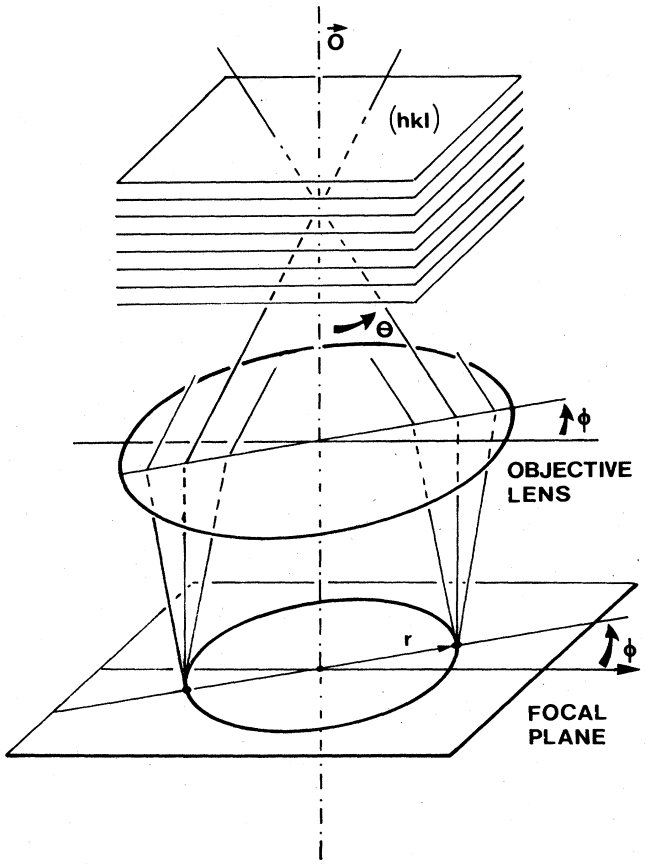

FIG. 5. Light paths in the sample.

The image of the crystal is then formed by rays Bragg reflected from (hkl) planes. The quality of this image and the resolution of a corresponding Bragg spectrum deteriorates rapidly when the aperature diaphragm is open because when a convergent beam illuminates the sample, other crystal planes $(h'k'l')$ oblique to **O** can also reflect incident rays. Let the direction of the rays be described by angles θ and ϕ (Fig. 5) and $\{(\theta,\phi)\}$ be a set of (parallel) beams reflected from (hkl) and $(h'k'l')$ planes. In the image plane of the objective each of those reflected beams gives rise to a different image of the crystal. The superposition of all these images introduces confusion and deteriorates the quality of visual information. On the other hand, each of the ray beams from the set $\{(\theta,\phi)\}$ is focused into a different point (θ,ϕ) in the focal plane of the objective. With the aperture diaphragm open, it is clearly more interesting to observe the focal plane of the objective rather than the image plane.

B. Experimental setup for the convergent beam technique

Most polarizing microscopes can be converted into a conoscope[6] by introduction of the so-called Bertrand lens between the objective and the eye piece. This additional lens forms an image of the focal plane of the microscope.[6] Unfortunately this option did not exist in the reflecting metallurgical microscope, used in our experimental setup shown in Fig. 6, and we adopted the following solutions. To directly observe (visually) the focal plane, we replaced the ordinary eye pieces by telescopes made of achromatic lenses L and the eye pieces. Lens L is here effectively a Bertrand lens. We used a standard photographic camera equipped with a long-focal (135 mm) objective (LFO) in order to take a photographic picture of the focal plane.

C. Kossel diagrams in BP I and BP X

The photographs shown in Fig. 7 were obtained as follows. In a sample with the concentration of CB15 $c=42.5\%$, large monocrystals of BP I were first grown from the isotropic liquid phase. Using the microscope in its orthoscopic[6] (normal) configuration, a large (≈ 30 μm in diameter) isolated monocrystal of a suitable orientation (see below) was selected and moved (using the microscope stage) into the center of the field. The diaphragm was then closed, the aperture diaphragm opened, and the eye pieces replaced by the telescope.

1. BP I, [110]||O, E=0

A typical conoscopic photograph of a BP I crystal with orientation [110]||**O**, shown in Fig. 7(a), reveals a very characteristic pattern of Kossel lines. Identical patterns have been observed previously, by a different technique, in bcc colloidal crystals[7] so we concluded that BP I has a bcc structure.

2. BP I→BP X transition

When an increasing electric field was applied to the sample, the Kossel pattern started to deform. In weak fields this deformation is not large but is obvious if one considers intersections of Kossel lines. For example, in Fig. 7(a) three Kossel lines of indices (200), (101), and $(10\bar{1})$ cross at one point. This kind of degeneracy is not accidental (depending on the wavelength of the illuminating beam) but characteristic of cubic symmetry. In a field this degeneracy is removed. Instead of crossing at one point, the lines now cross at three points making a triangle (cf. Fig. 10 where a series of corresponding theoretical

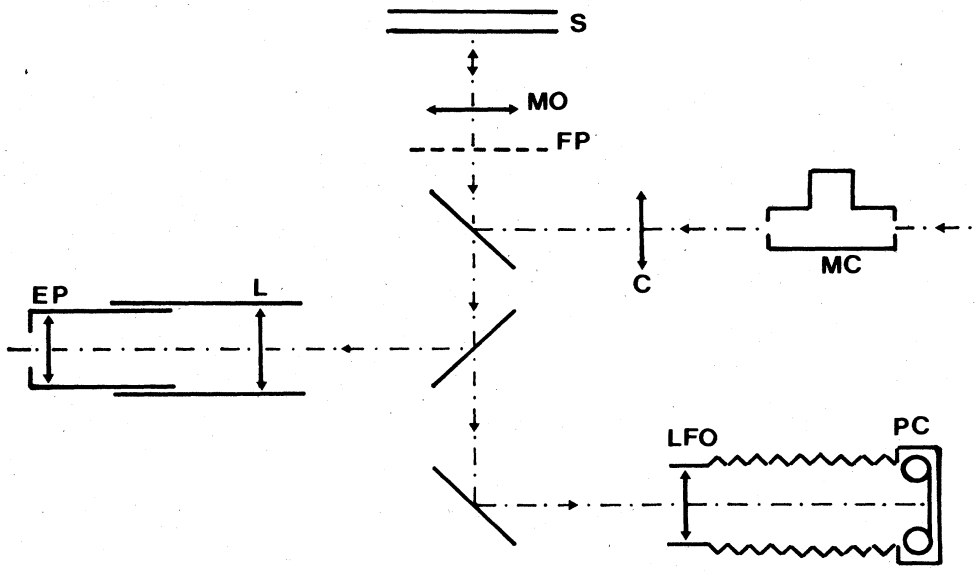

FIG. 6. Experimental setup (general view): S, sample; MO, microscope objective; FP, focal plane; C, condenser; MC, monochromater; EP, eye piece; L, lens; LFO, long-focal objective; PC, photographic camera.

diagrams are shown). The deformation of the Kossel diagram increases with the field but its twofold axis is preserved for $E < E_{I/X}$. At $E = E_{I/X}$ there is a rapid but still continuous change in conformation of Kossel lines and the Kossel diagram acquires fourfold symmetry [Figs. 7(c) and 7(d)].

IV. THE STRUCTURE OF BP X FROM ITS KOSSEL DIAGRAMS

We now have at our disposal observations in both direct and reciprocal space of changes in BP I monocrystals during the transition to BP X. Are the changes observed in the Kossel diagrams during the transition compatible with

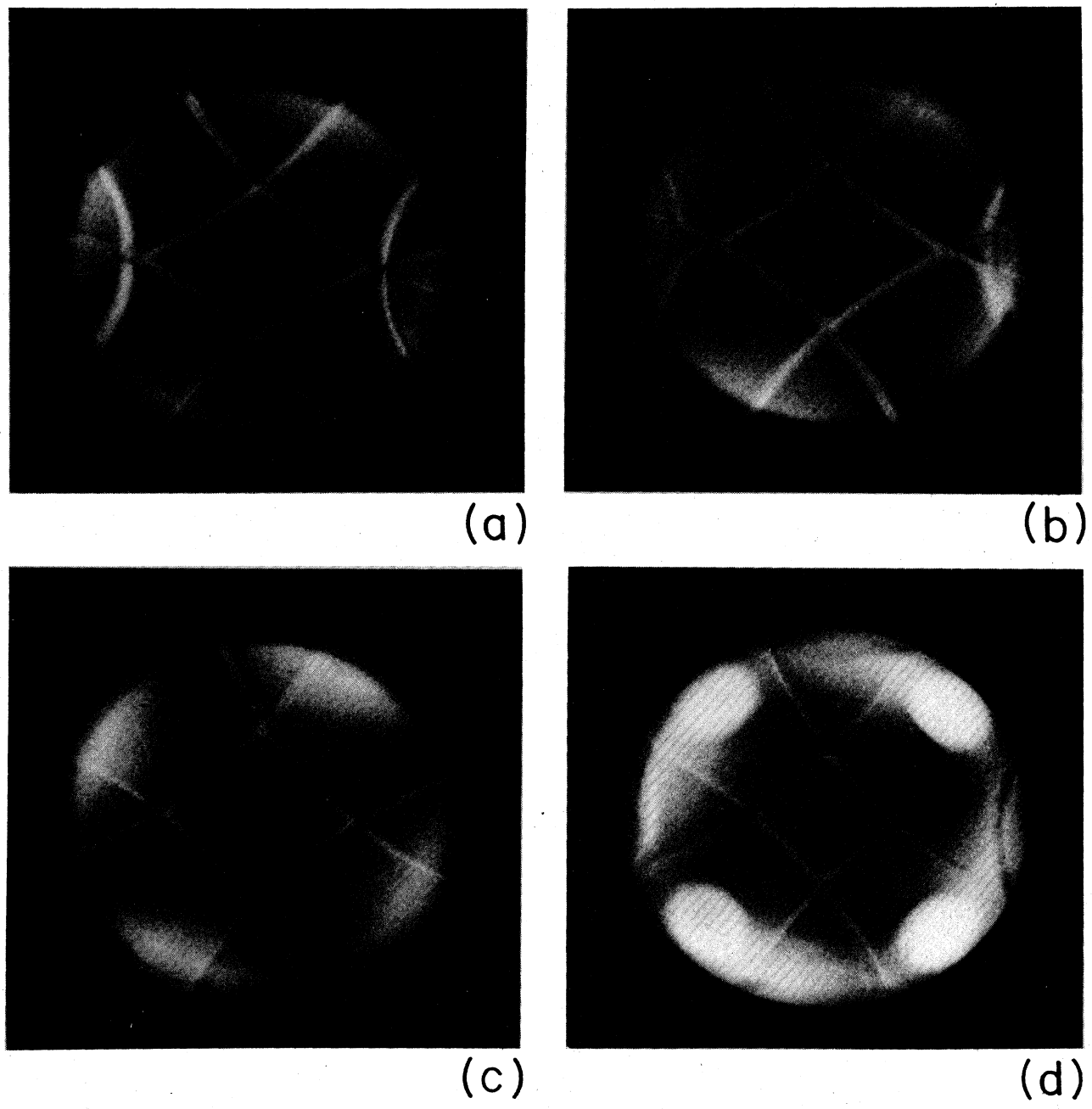

FIG. 7. Photographs of the focal plane of the objective: (a) $E = 0$, BP I; (b) $0 < E < E_{I/X}$; (c) $E = E_{I/X}$; (d) $E = E_{I/X}$. (a)—(c) $\lambda = 529$ nm, (d) $\lambda = 496$ nm. The sample is 42.5% CB15 in E9.

conclusion (5) in Sec. II which was based on direct observations of this transition? Our strategy to answer this question, crucial for understanding BP *X*, is to first consider how the reciprocal lattice is modified as a result of conclusion (5) deformations, then we reconstruct the Kossel diagrams of this modified reciprocal lattice and show that it is indeed consistent with observations.

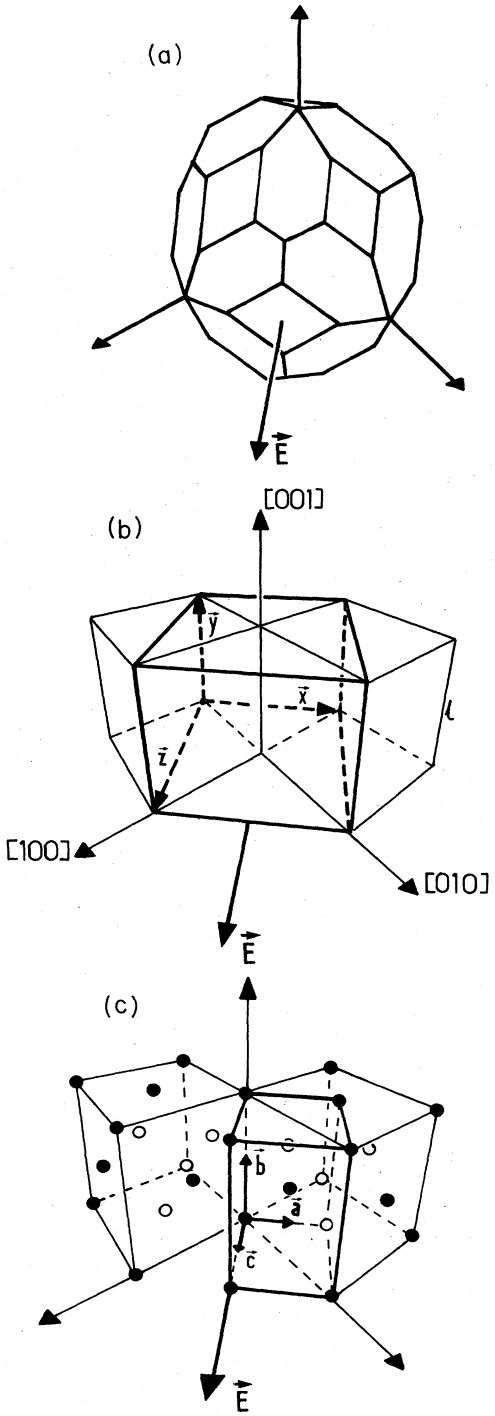

FIG. 8. (a) Orientation of a crystal of BP I with respect to axes **x**,**y**,**z** shown in (b). Choice of bases and of unit cells in direct space (b) and in reciprocal space (c). The field **E** is parallel to **z**.

A. Deformation of the bcc lattice in real space

Let **i**,**j**,**k** be orthogonal unit vectors parallel to $[\bar{1}10]$, [001], and [110] directions, respectively, of the BP I crystal shown in Fig. 8(a). Consider now an orthorhombic *F*-centered unit cell, instead of the cubic centered unit cell [Fig. 8(b)]. The edges adjacent to the origin of this orthorhombic unit cell can be represented by three vectors **x**,**y**,**z** given by

$$\begin{aligned} \mathbf{x} &= \sqrt{2}l\mathbf{i} , \\ \mathbf{y} &= l\mathbf{j} , \\ \mathbf{z} &= \sqrt{2}l\mathbf{k} . \end{aligned} \tag{1}$$

The deformation proposed in Fig. 3(b) consists of a superposition of an elongation of the crystal in the [001] direction and a contraction in $[\bar{1}10]$ direction. To be more general, we suppose that the crystal can also be deformed in the third direction [110]. Finally, we consider the crystal as incompressible. Under these conditions **x**,**y**,**z** change their lengths, but preserve their directions so that

$$\begin{aligned} \mathbf{x}' &= \alpha\sqrt{\beta}\mathbf{x} , \\ \mathbf{y}' &= \frac{\sqrt{\beta}}{\alpha}\mathbf{y} , \\ \mathbf{z}' &= \frac{1}{\beta}\mathbf{z} , \end{aligned} \tag{2}$$

where α is a parameter of the deformation in the (x,y) plane and β corresponds to an additional axial deformation in the direction of the field ($\mathbf{E}||\mathbf{z}||[110]$). Thus one finds easily that the orthorhombic cell $(\sqrt{2}l\times l\times\sqrt{2}l)$ is deformed into a tetragonal one $[(2)^{1/4}l\times(2)^{1/4}l\times\sqrt{2}l]$ for $\alpha=2^{-1/4}$ and $\beta=1$.

B. Deformation of the fcc lattice in reciprocal space

Consider now the reciprocal fcc lattice of BP I, shown in Fig. 8(c), with basis **a**,**b**,**c** reciprocal to **x**,**y**,**z**. One has

$$\begin{aligned} \mathbf{a} &= \frac{2\pi}{\sqrt{2}l}\mathbf{i} , \\ \mathbf{b} &= \frac{2\pi}{l}\mathbf{j} , \\ \mathbf{c} &= \frac{2\pi}{\sqrt{2}l}\mathbf{k} . \end{aligned} \tag{3}$$

In the crystal deformed following Eq. (2), these basis vectors become

$$\begin{aligned} \mathbf{a}' &= \frac{1}{\alpha\sqrt{\beta}}\mathbf{a} , \\ \mathbf{b}' &= \frac{\alpha}{\sqrt{\beta}}\mathbf{b} , \\ \mathbf{c}' &= \beta\mathbf{c} . \end{aligned} \tag{4}$$

The orthorhombic *I*-centered unit cell

$$\left[\frac{4\pi}{\sqrt{2}l}\times\frac{4\pi}{l}\times\frac{4\pi}{\sqrt{2}l}\right]$$

alternative to the cubic unit cell is deformed into a tetragonal one

$$\left[\frac{4\pi}{(2)^{1/4}l}\ \frac{4\pi}{(2)^{1/4}l}\ \frac{4\pi}{\sqrt{2}l}\right],$$

for $\alpha=2^{-1/4}$ and $\beta=1$.

Using the basis **a**,**b**,**c**, defined in Eq. (3), each point of the reciprocal lattice of BP I can be represented as

$$\mathbf{q}=h\mathbf{a}+k\mathbf{b}+l\mathbf{c}\ . \tag{5}$$

As the crystal deforms in the electric field, **q** becomes

$$\mathbf{q}'=h\mathbf{a}'+k\mathbf{b}'+l\mathbf{c}'\ , \tag{6}$$

where **a**′, **b**′, and **c**′ are vectors of the deformed base given by (4).

C. Principle of construction of Kossel diagrams

Knowing the reciprocal lattice of the crystal, the construction of the corresponding Kossel diagram is then straightforward. Let us consider the convergent light beam of wavelength λ illuminating the crystal (Fig. 5), and a family of lattice planes (hkl) corresponding to a vector **q** (hkl). Among all rays of the beam of direction defined in Fig. 5 by polar angles (θ,ϕ), those which satisfy the Bragg condition on (hkl) propagate differently (i.e., are backreflected) than all other rays which do not obey this condition.

Rays satisfying the Bragg condition form a cone of axis **q** (hkl) and angle

$$\delta\theta_{\mathbf{q}}=\arccos\frac{|\mathbf{q}|}{2q_0}\ , \tag{7}$$

where $q_0=2\pi n/\lambda$ is the wave vector in the sample of refractive index n. Obviously, Eq. (7) makes sense only if $|\mathbf{q}|<2q_0$ which means that **q** must be inside a sphere S of radius $2q_0$ (Fig. 9). Let $C_{\mathbf{q}}=\{(\theta,\phi)\}_{\mathbf{q}}$ be the set of rays in the (θ,ϕ) direction of the cone. In spherical coordinates θ,ϕ, defined on the sphere S, with the polar axis $\mathbf{z}||\mathbf{O}||\mathbf{E}$, the set $C_{\mathbf{q}}$ corresponds to a circle of angular radius given by Eq. (7) centered at $P(\theta_{\mathbf{q}},\phi_{\mathbf{q}})$ with coordinates

$$\theta_{\mathbf{q}}=\arccos(n_z),\quad n_z=\frac{1\,|\mathbf{c}|}{|\mathbf{q}|} \tag{8a}$$

$$\phi_{\mathbf{q}}=\arcsin(n_y/\sin\theta_{\mathbf{q}}),\quad n_y=\frac{k\,|\mathbf{b}|}{|\mathbf{q}|}\ . \tag{8b}$$

Each of the reciprocal lattice vectors **q** situated inside the sphere S gives rise to its own Kossel line on the sphere S and all such Kossel lines make up the Kossel diagram.

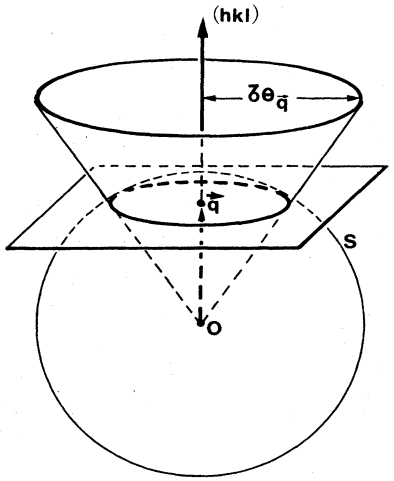

FIG. 9. Principle to construct Kossel diagrams.

D. Kossel diagrams of BP I→BP X transition. Discussion

The series of Kossel diagrams shown in Fig. 10 was obtained with the following choice of parameters.

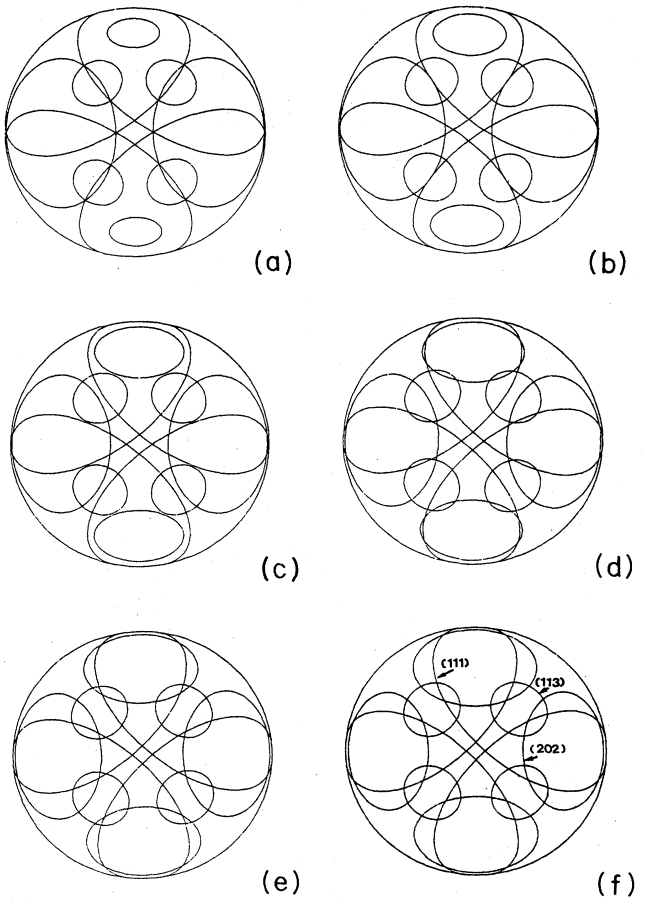

FIG. 10. Kossel diagrams of BP I progressively deformed into the BP X. (a) BP I, $E=0$; fcc reciprocal lattice: $\alpha_I=1$, $\beta=1$. (f) BP X, $E=E_{I/X}$, tetragonal F-centered reciprocal lattice: $\alpha_X=2^{-1/4}$, $\beta=1$. Configurations of Kossel diagrams for intermediate deformations $\alpha=1-n(1-2^{-1/4})/10$: (b) $n=2$, (c) 4, (d) 6, (e) 8. The patterns shown in Fig. 7 can be recognized in the central region of these drawings.

(1) The ratio $w=nl/\lambda$, which fixes relative dimensions of the sphere S and of the reciprocal lattice, was set to 1.25.

(2) With the above choice of w, the reciprocal lattice vectors situated inside the sphere S (in its "north hemisphere") have coordinates: (1,1,1), (1,$\bar{1}$,1), ($\bar{1}$,1,1), ($\bar{1}$,$\bar{1}$,1), (0,2,2), (0,$\bar{2}$,2), (2,0,2), ($\bar{2}$,0,2) (1,1,3), (1,$\bar{1}$,3), ($\bar{1}$,1,3), ($\bar{1}$,$\bar{1}$,3) in the base **a**,**b**,**c**.

(3) The parameter β was set arbitrarily to 1 while α was varied from 1 [Fig. 10(a)] to $2^{-1/4}$ (Fig. 10).

Several conclusions can be formulated from a comparison of these theoretical diagrams with the observed ones on Fig. 7. First of all it is clear that only a central segment of the sphere S of radius $\Delta\theta\approx 37°$ is effectively "visible" in the focal plane of the microscope. This effect is obviously due to a finite angular aperture of the microscope objective. Second, the transformation of this visible part of Kossel diagrams in Fig. 10 is in qualitative agreement with observations reported in Sec. III C. This confirms the tetragonal symmetry of BP X and answers the question posed at the beginning of Sec. IV. Finally, BP X can be obtained by a continuous deformation of BP I.

E. Aspect ratio of the tetragonal unit cell of the blue phase X

Although it is clear at this stage of our discussion that the unit cell of BP X is tetragonal, we are still ignorant of its aspect ratio $p=|\mathbf{Z}'|/|\mathbf{X}'|=|\mathbf{a}'|\,|\mathbf{C}'|$ which is equal to the height of the unit cell divided by the dimension of the square basis. In Sec. IV B by setting $\beta=1$ we fixed its value to $p_0=p(\beta=1)=2^{1/4}$.

In order to measure p, a dimensionless quantity, it is enough to measure angles in the Kossel diagrams. Let us consider, for example, the Kossel diagram of Fig. 7(d). Several angles such as θ_{113}, $\Delta\theta_{202}$, and $\Delta\theta_{111}$, defined in Fig. 11(a), can in principle be determined from the photograph in Fig. 7(d) provided that the relationship between the radius r in the plane of the photograph and the polar angle θ on the sphere S is known (see Fig. 5). We have realized the desired calibration using Fabry-Perot fringes produced by multiple reflections between the glass plates S_a and S_b. Using this calibration we found from Fig. 7(d)

$$\theta^m_{113}=31°\pm 1°\,, \tag{9a}$$

$$\Delta\theta^m_{202}=31°\pm 1°\,, \tag{9b}$$

$$\Delta\theta^m_{111}=8°\pm 1°\,. \tag{9c}$$

Theoretically, these angles are functions of the aspect ratio p and can be calculated as follows.

θ_{113}. In the photograph of Fig. 7(d) the wavelength λ of the illuminating beam was chosen in a way to obtain (113) Kossel rings of very small diameter. In terms of the construction shown in Fig. 9 it means that the radius $R_s=2q_0$ of the sphere S in the reciprocal space equals the length $|\mathbf{q}(113)|$ of the vector (113) in the reciprocal lattice. In the basis $\mathbf{a}',\mathbf{b}',\mathbf{c}'$, this length is

$$R_s=|\mathbf{q}(113)|=[(3|\mathbf{c}'|)^2+2(\mathbf{a}')^2]^{1/2} \tag{10a}$$

or, using the aspect ratio P, one has

$$R_s=|\mathbf{q}(113)|=|\mathbf{c}'|(9+2P^2)^{1/2}\,. \tag{10b}$$

The angle $\theta^{\rm th}_{113}$ is then given by Eq. (8),

$$\theta^{\rm th}_{113}=\arccos\frac{3}{(9+2p^2)^{1/2}}\,. \tag{11}$$

$\Delta\theta_{202}$ and $\Delta\theta_{111}$. The vectors $\mathbf{q}(202)$ and $\mathbf{q}(111)$ of respective lengths,

$$\mathbf{q}(202)=|\mathbf{c}'|(4+4p^2)^{1/2} \tag{12a}$$

and

$$\mathbf{q}(111)=|\mathbf{c}'|(1+2p^2)^{1/2}\,, \tag{12b}$$

are situated inside the sphere S. From Eqs. (7), (10), and (12) one gets

$$\delta\theta_{202}=\arccos\frac{(4+4p^2)^{1/2}}{(9+2p^2)^{1/2}} \tag{13a}$$

and

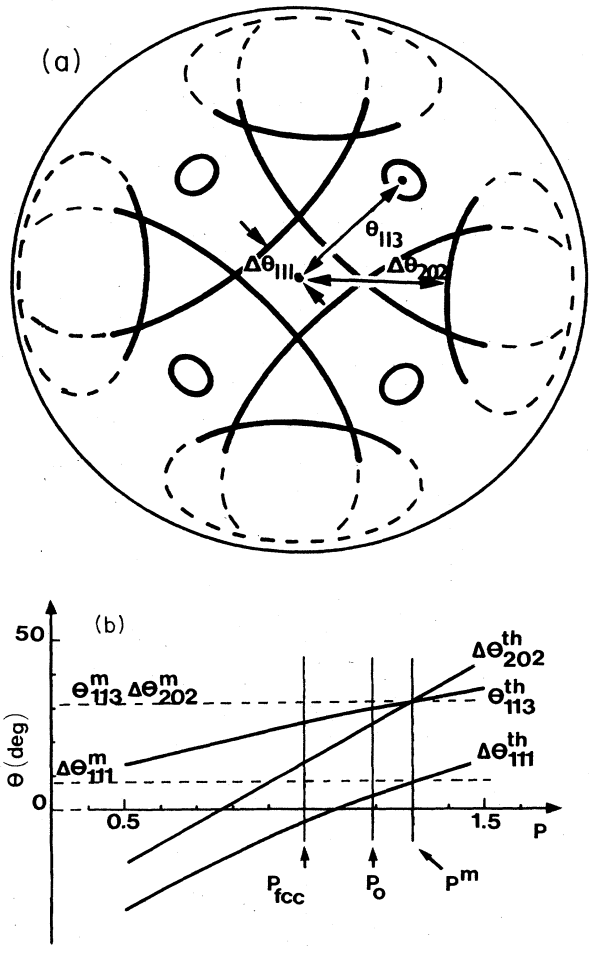

FIG. 11. Determination of the aspect ratio p of the tetragonal unit cell from the Kossel diagram: (a) definition of angles θ_{113}, $\Delta\theta_{202}$, and $\Delta\theta_{111}$; (b) determination of p from plots $\theta^{\rm th}_{113}$, $\Delta\theta^{\rm th}_{202}(p)$, and $\Delta\theta^{\rm th}_{111}(p)$.

$$\delta\theta_{111}=\arccos\frac{(1+2p^2)^{1/2}}{(9+2p^2)^{1/2}} . \tag{13b}$$

Similarly, from the Eqs. (8) and (12) one obtains

$$\theta_{202}=\arccos\frac{2}{(4+4p^2)^{1/2}} , \tag{14a}$$

$$\theta_{111}=\arccos\frac{1}{(1+2p^2)^{1/2}} . \tag{14b}$$

The desired angles $\Delta\theta_{202}$ and $\Delta\theta_{111}$ are then following functions of p:

$$\Delta\theta^{\text{th}}_{202}=\arccos\frac{2}{(4+4p^2)^{1/2}}-\arccos\frac{(4+4p^2)^{1/2}}{(9+2p^2)^{1/2}} \tag{15a}$$

and

$$\Delta\theta^{\text{th}}_{111}=\arccos\frac{1}{(1+2p^2)^{1/2}}-\arccos\frac{(1+2p)^{1/2}}{(9+2p^2)^{1/2}} . \tag{15b}$$

The measured values are compared with the theoretical ones in Fig. 11(b). The aspect ratio $p^m=1.3\pm0.02$, corresponding to the best fit, is larger than $p_0=p(\beta=1)=2^{1/4}=1.19$. It means that during BP I$\rightarrow$BP X transition the unit cell, defined in Fig. 8(b), elongates in the direction of the field. The parameter β^{-1}, which measures this elongation, is

$$\frac{1}{\beta}=\left[\frac{p^m}{2^{1/4}}\right]^{2/3}=1.061 . \tag{16}$$

V. DISCUSSION AND CONCLUSIONS

The conjecture, formulated in Ref. 2 on the existence of a uniaxial blue phase of tetragonal symmetry induced by electric fields has been demonstrated in the present paper in the direct and reciprocal spaces. This new blue phase has been shown to have the following principal features:

(a) its Bravais lattice in real space is centered tetragonal,

(b) its tetragonal axis is a screw axis 4_1,

(c) it can be obtained from BP I by a continuous deformation consisting of a shear in the plane perpendicular to the tetragonal axis, and of an elongation in the field direction,

(d) it can also be obtained from BP II by a discontinuous transformation whose nature has not been elucidated.

Among all space groups of the tetragonal system only one—D_4^{10} ($I4_122$ or $F4_122$)—is compatible with (a) and (b). From the point of view of symmetry, the property (c) means that for $0<E<E_{I/x}$, the symmetry of the blue phase is "intermediate" between O^8 ($I4_132$) and D_4^{10} ($I4_122$). A possible assignation of this intermediate symmetry is D_2^7 ($F222$); as required, the Bravais lattice is orthorhombic F-centered [Fig. 8(b)] and only twofold symmetry axes persist. In conclusion, the following sequence of symmetries are proposed:

$$\text{BP I}(O^8)\xrightarrow{E\neq0} D_2^7 \xrightarrow{E=E_{I/X}} \text{BP } X(D_4^{10}) .$$

The proposed symmetry of BP X also explains the discontinuous character of the BP II-BP X transition. The symmetry of BP II is O^2 ($P4_232$) and its Bravais lattice is simple cubic. Such a lattice cannot be transformed into a tetragonal F-centered lattice by a continuous deformation. In terms of space group symmetries it means that in the following sequence

$$\text{BP II}(O^2)\xrightarrow{E\neq0} D_4^5 \Longrightarrow \text{BP } X(D_4^{10}) ,$$

the second transition must be first order.

As final evidence that indeed we have observed an electric-field-induced structural transition and not a tetragonal distortion of the cubic phase, we define order parameters η_1 and η_2 to describe the tetragonal-orthorhombic transition. η_1 and η_2 are defined in general as components of a deformation tensor e_{ij} of the tetragonal unit cell.[8] When z is parallel to the fourfold axis, $\eta_1=e_{xx}-e_{yy}$ and $\eta_2=e_{xx}+e_{yy}-2e_{zz}$. In the tetragonal phase, $E>E_{I/X}$, $\eta_1=0$. At $E_{I/X}$ the 422 point symmetry of the tetragonal phase is broken and replaced by the 222 symmetry of the orthorhombic phase so $\eta_1\neq0$. The free energy F_1 is even in η_1 by symmetry:

$$F_1=\alpha\eta_1^2+B_0\eta_1^4+\cdots . \tag{17}$$

At $E_{I/X}$, $\alpha=0$. Here the analogue of temperature is E and α is the elastic constant $(C_{11}-C_{12})/4$. The energy to distort the unit cell in the direction parallel to the field is

$$F_2=F_0+\frac{1}{2\chi}\eta_2^2 . \tag{18}$$

Here, $1/2\chi$ is the elastic constant

$$\frac{(C_{11}+C_{12}-4C_{13}+2C_{33})}{9} .$$

Because η_2 is an invariant of the 422 group, there is a coupling between the two order parameters η_1 and η_2 that to lowest order is of the form

$$F_{12}=-\Gamma\eta_1^2\eta_2,\quad \Gamma>0 . \tag{19}$$

The total energy $F=F_1+F_2+F_{12}$ is now seen to be identical to the familiar[9] nematic—smectic-A transition when the layer order parameter, ψ, is coupled to the orientational order parameter S; or, the Bean-Rodbell magnetic transition, where magnetization is coupled to lattice deformations.[10] In our case η_1 is analogous to ψ/magnetization and η_2 to S/lattice deformations. As de Gennes has shown,[9] the presence of F_{12} renormalizes the coefficient of the fourth-order term to $B=B_0-\chi\Gamma^2/2$. Thus B may be negative for large enough χ and Γ.

A negative B, of course, means that the transition is first order and higher order terms must be included in Eq. (17). Bean and Rodbell[10] have explicitly calculated a parameter proportional to $1-B$.

η_1 is measured directly from the Kossel diagrams by measuring $\cot\xi_4$, where $\cot\xi_4$ is defined in the following way. Each of the larger Kossel rings begins and ends on the boundary of the visible part of the focal plane. Draw a line joining these two end points. Then ξ_4 is the angle between this line and the horizontal line that bisects the

figure; $\cot\xi_4 = 1+\eta_1$. ξ_4 measures the ratio of the two sides of the [110] face. For a bcc crystal $\cot\xi_4 = \sqrt{2}$. We find $\cot\xi_4 = 1.43$ when $E = 0$ within experimental error. Comparing the variation with field of $\eta_1 = \cot\xi_4 - 1$ in Fig. 12 with their theoretical estimates for the magnetization as a function of temperature, the tetragonal-orthorhombic transition seems weakly first order. B is slightly negative or the Bean-Rodbell parameter is about 1.3.

The occurrence of the tetragonal phase has the following important implication on BP I structures. While the fundamental idea[11,12] that double twist relieves cholesteric frustration is indisputable, detailed models with extended objects like double twist cylinders threading many unit cells[13] may not be the building block of BP I. The reason is that an O^8 model built of rigid double twist cylinders cannot be deformed to a structure with fourfold symmetry without breaking cylinders. With the deformation we have described, its twofold axis remains a twofold axis.

Our main conclusion is that we have observed an electric field induced structural phase transition. The field is applied along a twofold direction of the crystal that transforms to the fourfold direction of the tetragonal crystal. Since the [110] direction maintains its twofold symmetry right up to the transition (Fig. 7), we can exclude rigid rotation of the crystal as a cause for the fourfold pattern at E_c. Rotation of the crystals is also excluded by direct observation. They deform but do not rotate in the field. Additional evidence that the structure has indeed undergone a phase transition to the tetragonal phase is found when the fct monocrystal transforms back to the distorted cubic phase. When the field is decreased below E_c, in general domains separated by grain boundaries corresponding to *both* signs of η_1 occur. One domain may eventually be favored and a bcc monocrystal is again recovered.

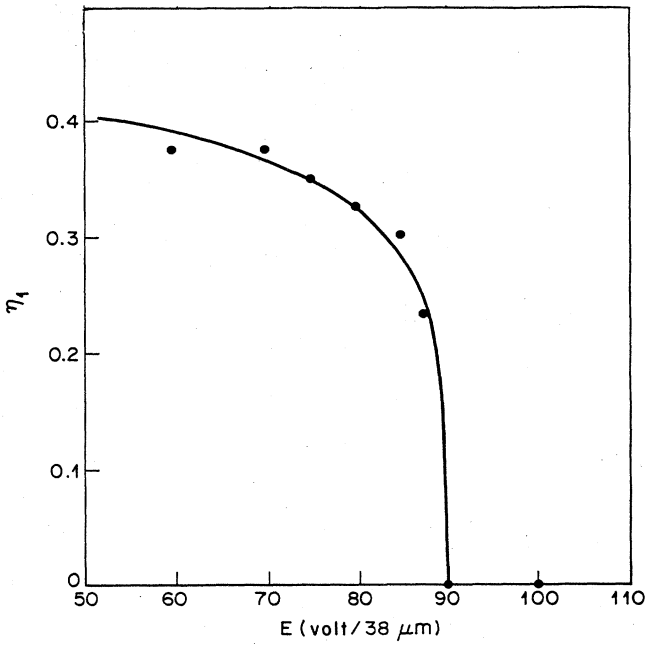

FIG. 12. Variation of the elastic order parameter η_1 as a function of electric field.

ACKNOWLEDGMENTS

P.E.C. thanks Physique des Solides, Orsay for kind hospitality and support during this work. We thank M. Gabay, F. Rothen, J. Sethna, and D. Rokhsar for interesting discussions. The Laboratoire de Physique des Solides is Laboratoire associé au Centre National de la Recherche Scientifique.

[1]R. M. Hornreich, H. Kugler, and S. Shtrikman, in Proceedings of the Winter Workshop on Colloidal Crystals [J. Phys. (Paris) Colloq. **46**, C3-47 (1985)].

[2]P. Pieranski, P. E. Cladis, and R. Barbet-Massin, J. Phys. (Paris) Lett. **46**, L-973 (1985). CB15 is a British Drug House designation for chiral 4-cyano-4′-(2-methyl)butylbiphenyl. E9 is a British Drug House designation for a eutectic mixture of three or more 4-cyano-4′-(*n*-hexyloxy)biphenyl (with $n = 3$, 5, and 7) and 4-cyano-4′-(*n*-pentyl)triphenyl.

[3]P. Pieranski and B. Pansu, in Proceedings of the Winter Workshop on Colloidal Crystals [J. Phys. (Paris) Colloq. **46**, C3-281 (1985)].

[4]G. Heppke, M. Krumrey, and F. Oestreicher, Mol. Cryst. Liq. Cryst. **99**, 99 (1983).

[5]M. Marcus, Phys. Rev. A **25**, 2272 (1982).

[6]E. E. Wahlstrom, *Optical Crystallography*, 4th ed. (Wiley, New York, 1969).

[7]P. Pieranski, E. Dubois-Violette, F. Rothen, and L. Strzelecki, J. Phys. (Paris) **42**, 53 (1981).

[8]See, for example, N. Boccara, Ann. Phys. (N.Y.) **47**, 40 (1968).

[9]P. G. de Gennes, *The Physics of Liquid Crystals* (Clarendon, Oxford, 1979), p. 327.

[10]C. P. Bean and D. S. Rodbell, Phys. Rev. **126**, 104 (1962).

[11]J. P. Sethna, Phys. Rev. B **31**, 6278 (1985).

[12]S. Meiboom, J. Sethna, P. W. Anderson, and W. F. Brinkman, Phys. Rev. Lett. **46**, 1216 (1981).

[13]S. Meiboom, M. Sammon, and D. W. Berreman, Phys. Rev. A **28**, 3553 (1983).

[14]G. Heppke, H. S. Kitzerow, and M. Krumrey (private communication).

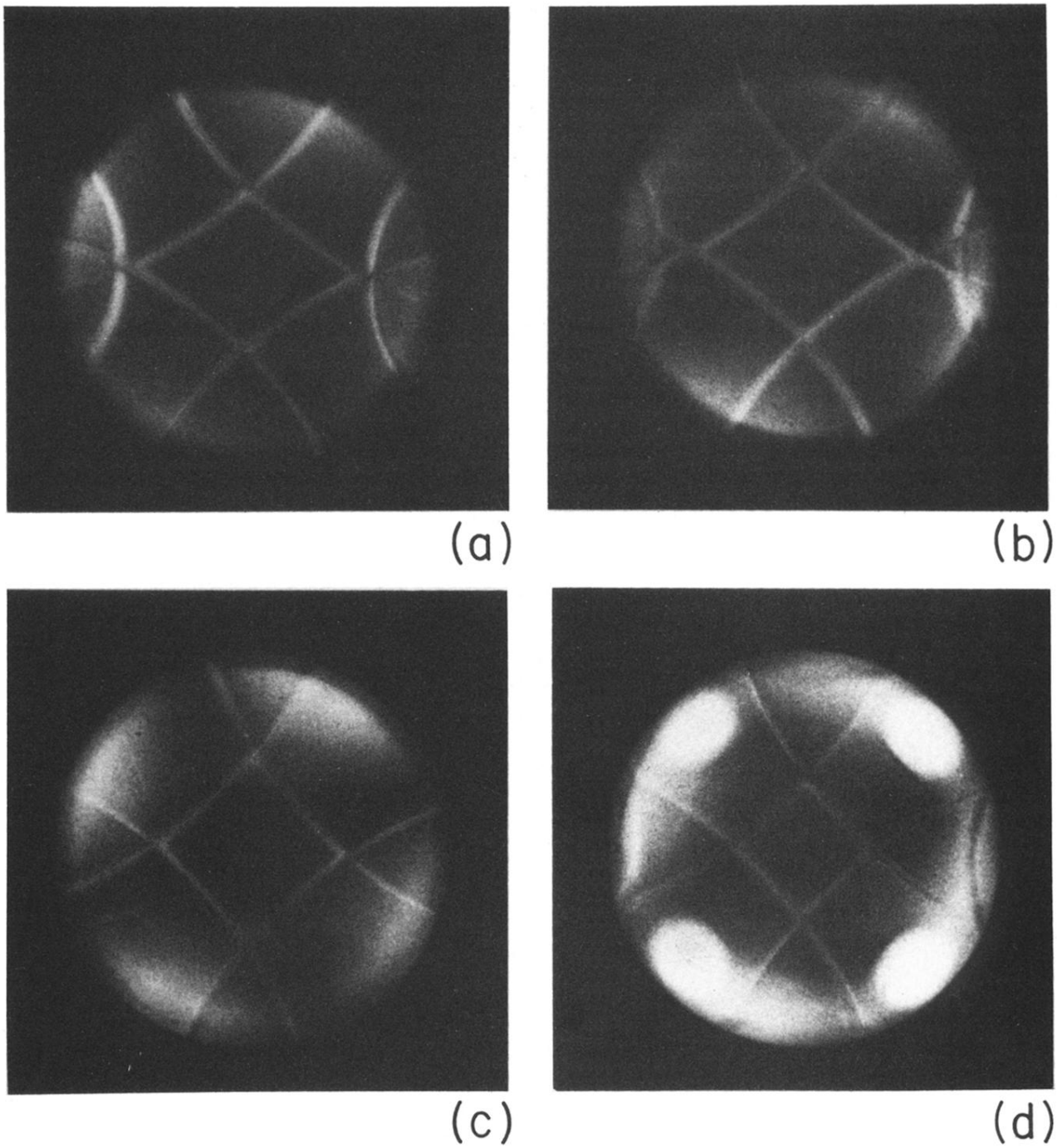

FIG. 7. Photographs of the focal plane of the objective: (a) $E=0$, BP I; (b) $0<E<E_{I/X}$; (c) $E=E_{I/X}$; (d) $E=E_{I/X}$. (a)–(c) $\lambda=529$ nm, (d) $\lambda=496$ nm. The sample is 42.5% CB15 in E9.